

## Design and Properties of Ni-TiN/SiC Nanocoatings Prepared by Pulse Current Electrodeposition

Fafeng Xia<sup>1,2</sup>, Qiang Li<sup>1</sup>, Chunyang Ma<sup>1,\*</sup>, Danqiong Zhao<sup>1</sup>, Zhipeng Ma<sup>1</sup>

<sup>1</sup> College of Mechanical Science and Engineering, Northeast Petroleum University, Daqing 163318, China;

<sup>2</sup> College of Mechanical and Electrical Engineering, Hohai University, Changzhou, 213022, China

\*E-mail: [chunyangandma1@163.com](mailto:chunyangandma1@163.com)

Received: 25 September 2019 / Accepted: 9 November 2019 / Published: 31 December 2019

---

Ni-TiN/SiC nanocoatings were fabricated using pulse current electrodeposition (PCE) technique. The influence of plating parameters on morphology, microstructure, microhardness, and wear behavior of the resulting coatings were investigated by instrumental techniques such as transmission electron microscopy (TEM), scanning electron microscopy (SEM), X-ray diffraction (XRD) and X-ray photoelectron spectroscopy (XPS) as well as by tribological, abrasion and electrochemical testing. Test results confirmed incorporation of numerous TiN and SiC nanoparticles (with 45.9 and 37.2 nm average sizes, respectively) into the coating prepared at 4 A/dm<sup>2</sup> pulse current density. Cross-sectional views of this nanocoating revealed high concentrations of Ti (19.6 at%), Si (12.1 at%), and Ni (53.3 at%). Microhardness of this Ni-TiN/SiC nanocoating was 848.1 Hv, which is significantly higher comparing to other coatings prepared in this work. The wear rate of Ni-TiN/SiC nanocoating prepared at 4 A/dm<sup>2</sup> was only 13.6 mg/min, and only some small surface scratches were observed. Both of these results indicate outstanding wear resistance and performance of our novel Ni-TiN/SiC nanocoatings. In addition, Ni-TiN/SiC nanocoating deposited at 4 A/dm<sup>2</sup> had the smallest corrosion current density equal to 8.12×10<sup>-6</sup> A/cm<sup>2</sup>, which indicates the best corrosion resistance.

---

**Keywords:** Ni-TiN/SiC nanocoating; pulse current electrodeposition; microstructure; microhardness; wear resistance

### 1. INTRODUCTION

Recently, metal-based ceramic composite coatings (consisting of Ni-TiN, Ni-AlN, Ni-Co/SiC, and Ni-CeO<sub>2</sub> composites) attracted a lot of attention because of their excellent physical and chemical properties, such as microhardness, wear and thermal resistance [1-10]. These composite coatings can be prepared using electrodeposition, electroless plating, and brush plating techniques [11-13]. Comparing to electroless and/or brush plating, electrodeposition processes several advantages such as high

deposition rates, coatings with simpler structures, no limitations for reinforcing particle composition and reduced electrode losses.

Depending on the current source, electrodeposition can be divided into two categories: direct and pulse current electrodeposition (DCE and PCE, respectively). PCE offers faster plating rates and is often used in petroleum and chemical industries because it produces coatings with decreased internal stresses and porosity as well as finer matrix grains [14-17].

TiN and SiC particles are inorganic ceramic materials. TiN nanoparticles, because of their high hardness and strength as well as outstanding wear and corrosion resistance, are often used as reinforcing materials to produce coatings with enhanced physical and chemical properties [18-20]. SiC nanoparticles also possess high microhardness and thermal stability as well as outstanding wear resistance. Therefore, we attempted to simultaneously incorporate TiN and SiC nanoparticles into a metal-based ceramic composite coating to obtain improved physical and chemical characteristics. We also assessed how electroplating parameters affect morphology, microstructure, microhardness, wear behavior and corrosion resistance of the as-fabricated Ni-TiN/SiC nanocoatings.

## 2. EXPERIMENT

Ni-TiN/SiC nanocoatings were prepared using PCE and Q235 steel as a substrate. Modified plating solution contained 200 g/L NiSO<sub>4</sub>, 30 g/L NiCl<sub>2</sub>, 30 g/L H<sub>3</sub>BO<sub>3</sub>, 60 mg/L cetyltrimethylammonium bromide, 8 g/L TiN nanoparticles, and 8 g/L SiC nanoparticles [21]. The diameters of initial TiN and SiC nanoparticles ranged from 20 to 40 nm. Nickel plate (30×30×10 mm) served as an anode, and 30×20×5 mm Q235 steel plate served as a cathode. Electrodes were positioned 200 mm apart. Experimental setup contained a pulse current source (SMD-100), heating system (DRB-1000), ultrasonic agitator (XL-300), and a plating bath (see Fig. 1). Current densities during PCE were 2, 4 and 6 A/dm<sup>2</sup> at 40% duty cycle. The temperature of the plating solution was maintained at 45°C. TiN and SiC nanoparticles were continuously ultrasonicated in the plating solution, pH value of which was maintained at 4.6. Plating time was 40 min. After PCE, the electrodes were cleaned ultrasonically for 10 min to remove loosely adsorbed TiN and SiC nanoparticles.

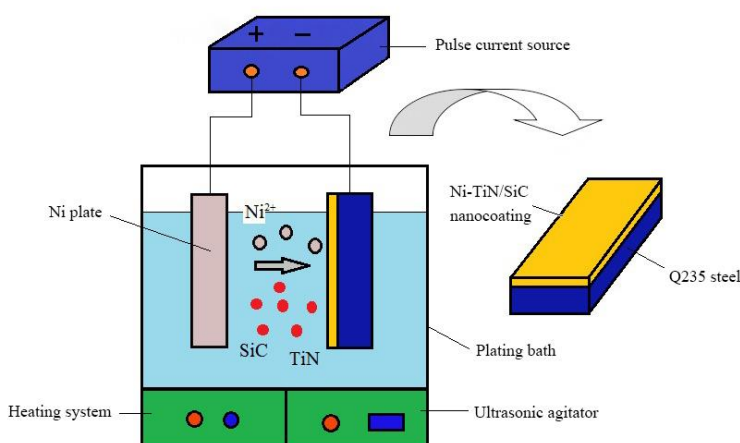


**Figure 1.** Experimental device for preparing Ni-TiN/SiC nanocoatings.

The surface morphologies, cross-sections, and microstructures of the as-obtained Ni-TiN/SiC nanocoatings were examined using transmission electron microscopy (TEM, Tecnai-G2-20-S-Twin) and scanning electron microscopy (SEM, S3400) equipped with IE-300X energy dispersive spectroscopy (EDS). The phase composition of the coating surface was determined by Rigaku D/Max-2400 X-ray diffraction (XRD) using Cu-K $\alpha$  radiation ( $k=1.54 \text{ \AA}$ ), while cross-sectional compositions were analyzed by X-ray photoelectron spectroscopy (XPS, INCA X-MAX). Nano-hardness values were measured by TI-950 tribo-indenter at a 10 s 1000  $\mu\text{N}$  loading force. Friction and wear tests were performed using MRH-6 abrasion tester (Jingchen Test Instrument, China). Hardened steel barrel (GC15) was applied to the nanocoating surface at 5 N of applied load and 0.1 m/s constant speed under dry sliding conditions at room temperature (Fig. 2). Wear test lasted 30 min, after which the worn surfaces were analyzed by SEM. The wear rate ( $V$ ) of each coating was calculated based on Eq. (1):

$$V = \frac{M1 - M2}{L} \quad (1)$$

where  $M1$  and  $M2$  are sample weights before and after a wear test (measured with 0.1 mg accuracy), respectively, and  $L$  is a sliding length of the steel ball during wear experiments.

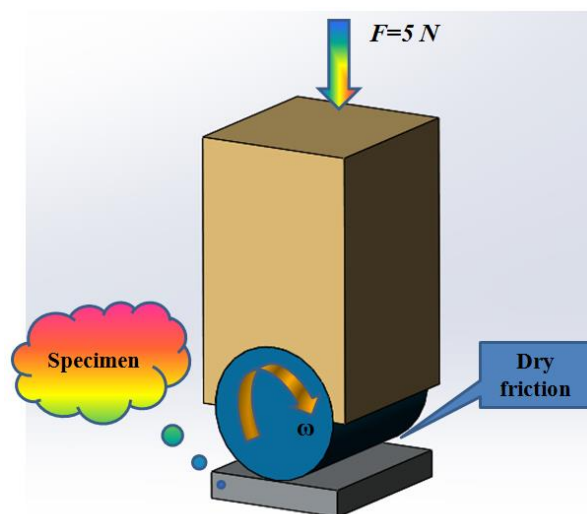


**Figure 2.** The friction experiment diagram for measuring the wear properties of Ni-TiN/SiC nanocoatings.

Electrochemical corrosion tests were performed by a CS350 electrochemical workstation using a 3.5 wt.% NaCl etching solution. Room temperature potentiodynamic polarization curves were recorded at 3 Hz and 2 mV/s scan rate. Nyquist plots were collected at open circuit potential equal to 10 mV.

### 3. RESULTS AND DISCUSSION

#### 3.1 TiN and SiC nanoparticles

TiN and SiC (with average diameters equal to 40 and 35 nm, respectively) were somewhat aggregated very likely because of their small sizes [23]. However, they were crystalline as shown in see Fig. 3.

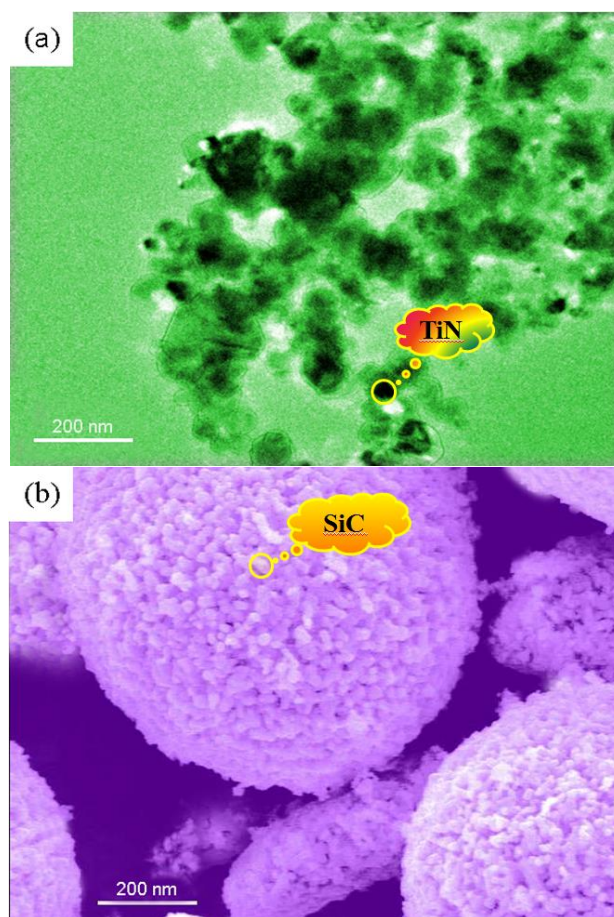


**Figure 3.** TEM images of TiN and SiC products: (a) TiN nanoparticles, and (b) SiC nanoparticles.

### 3.2 SEM analysis

Figure 4 illustrates surface and cross-sectional morphologies of Ni-TiN/SiC nanocoatings prepared at 2, 4 and 6 A/dm<sup>2</sup> pulse current densities. At 2 A/dm<sup>2</sup>, large grains with uneven and coarse structures formed on the Ni-TiN/SiC coating surface (see Figure 4a). At 4 A/dm<sup>2</sup>, Ni-TiN/SiC nanocoating demonstrated smooth and uniform surface with fine texture (see Figure 4b). As the pulse current density was increased to 6 A/dm<sup>2</sup>, the grain size of the Ni-TiN/SiC nanocoating increased (see Figure 4c). Thickness of the Ni-TiN/SiC nanocoating increased from 46.8 to 58.7  $\mu\text{m}$  as pulse current density was increased from 2 to 6 A/dm<sup>2</sup> (Fig. 4a'-c'). Thus, pulse current density significantly affected surface morphology, grain structure, and thickness of Ni-TiN/SiC nanocoatings.

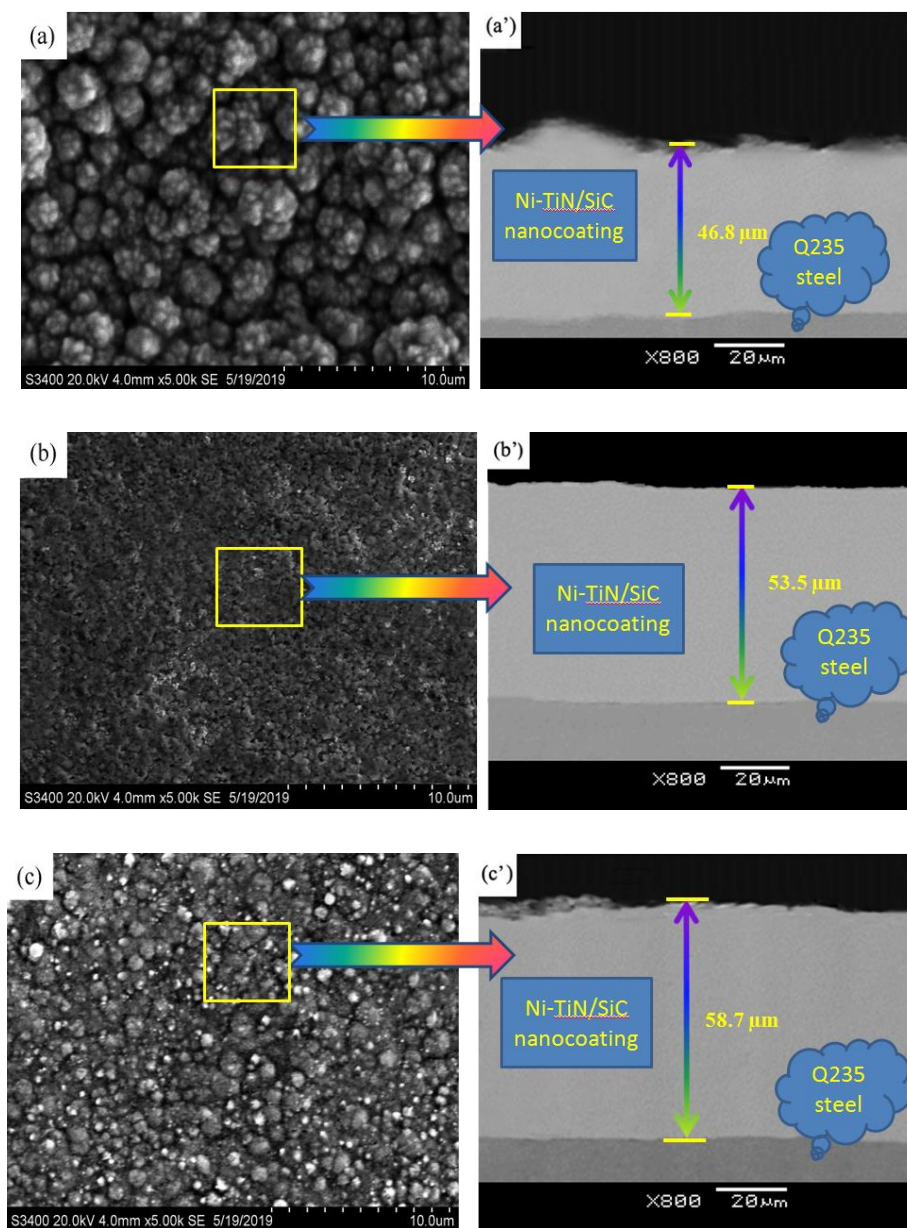


**Figure 4.** SEM images of Ni-TiN/SiC nanocoatings prepared with different pulse current densities: (a) 2 A/dm<sup>2</sup>, (b) 4 A/dm<sup>2</sup>, and (c) 6 A/dm<sup>2</sup>.

### 3.3 TEM

Fig. 5 shows TEM micrographs of Ni-TiN/SiC nanocoatings prepared at different pulse current densities. The black sections in Fig. 5a-c show TiN and SiC nanoparticles, whereas the white sections are Ni grains. When the composite coating was prepared at 2 A/dm<sup>2</sup>, TiN and SiC nanoparticles appeared only on the surface of the coating, while at 4 A/dm<sup>2</sup> TiN and SiC nanoparticles (with average diameters equal to 45.9 and 37.2 nm) were observed only inside the coating.

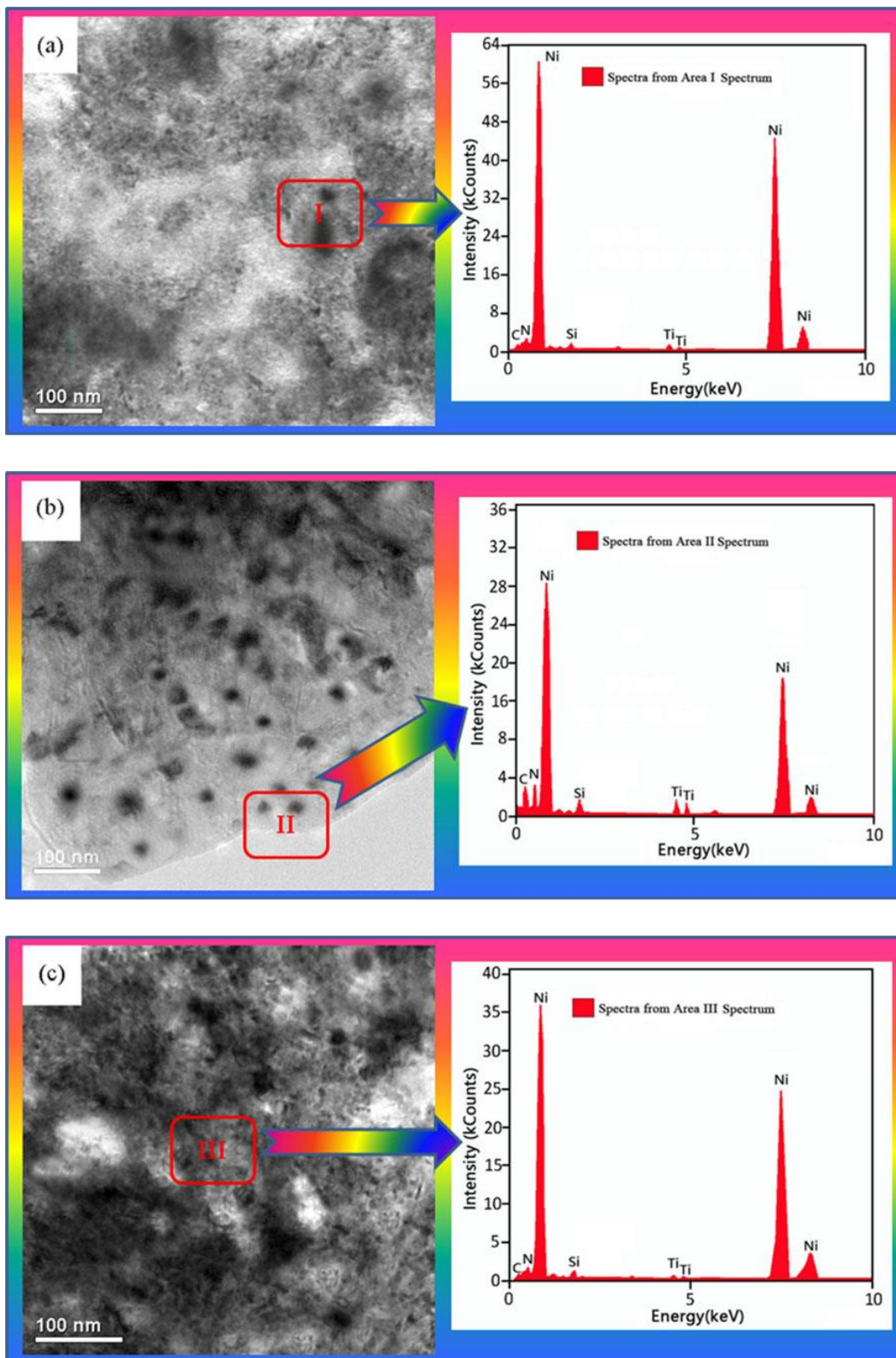


**Figure 5.** TEM micrographs of Ni-TiN/SiC nanocoatings prepared with different pulse current densities: (a) 2 A/dm<sup>2</sup>, (b) 4 A/dm<sup>2</sup>, and (c) 6 A/dm<sup>2</sup>.

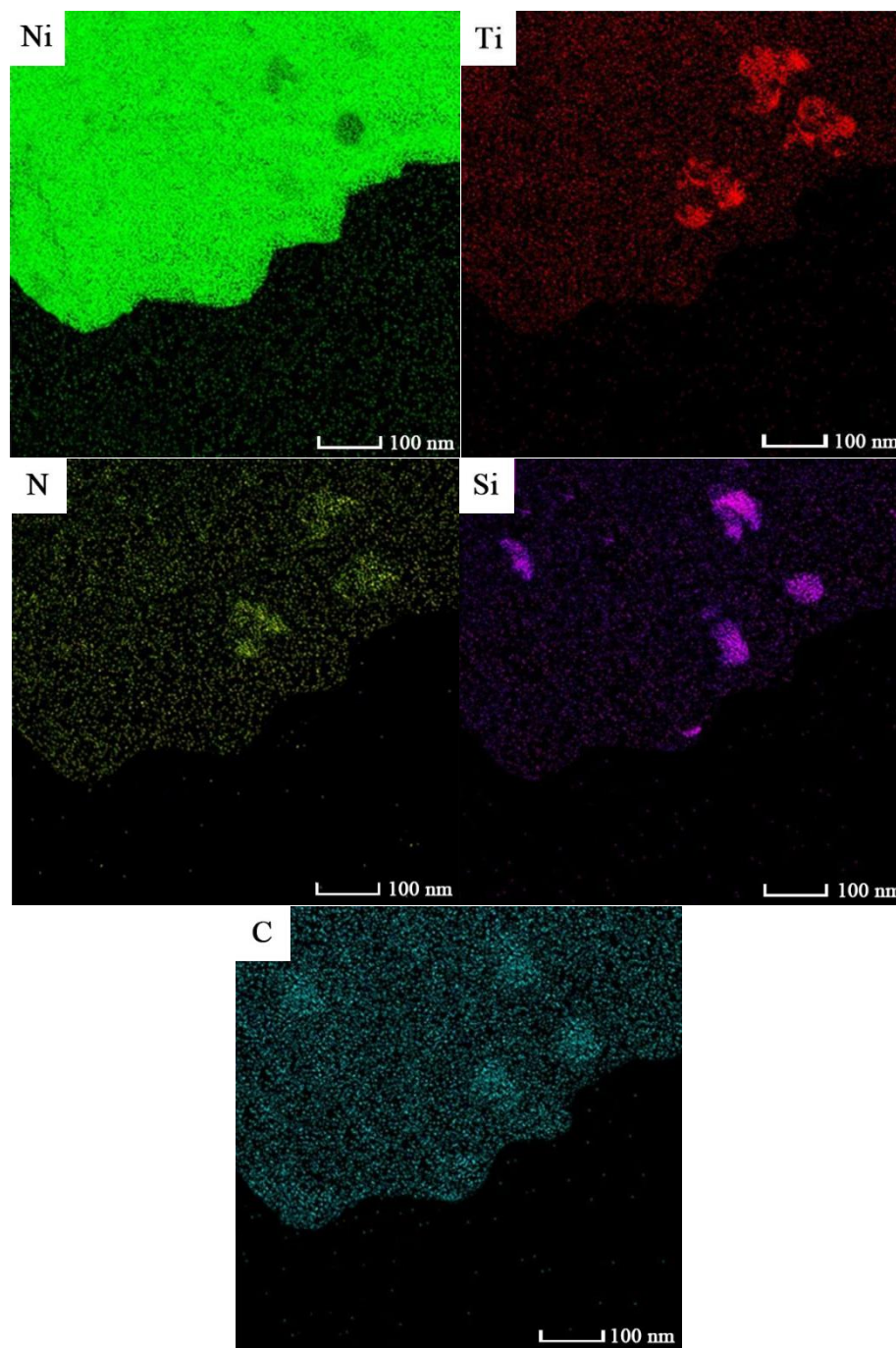


**Figure 6.** TEM bright field image of Ni-TiN/SiC nanocoating deposited at pulse current density of 4 A/dm<sup>2</sup>.

We believe that insufficient pulse current density (such as 2 A/dm<sup>2</sup>) prevented the incorporation of TiN and SiC nanoparticles into the coating. Ni-TiN/SiC coating deposited at 6 A/dm<sup>2</sup> demonstrated very large Ni grains and numerous agglomerated TiN and SiC nanoparticles.

Bright-field TEM micrographs showed homogeneous distribution of Ni, Ti, Si, N, and C in the Ni-TiN/SiC nanocoating prepared at 4 A/dm<sup>2</sup> (see Fig. 6), which confirms successful incorporation of TiN and SiC nanoparticles into the Ni matrix.

### 3.4 Co-deposition mechanism

The schematic presentation of the co-deposition mechanism of Ni, TiN, and SiC during PCE is shown in Fig. 7. Guglielmi's theory describes the occurring processes best. Ni ions present in the plating solution are first adsorbed by TiN and SiC nanoparticles, which then move toward the cathode under the applied electric field force ( $F$ ). Meanwhile,  $H_2$  forms at the cathode. TiN and SiC nanoparticles diffuse through both electric double and hydrogen evolution layers into the Ni matrix. This results have been confirmed by Lan [24], Li [25], and Bahadormanesh [26]. It is obvious that the electrolyte composition and electric field force have great influence on the content of TiN and SiC nanoparticles in Ni-TiN/SiC nanocoatings.

As is known to all, the pulse current density shows notable influence on the distribution and amount of embedded TiN and SiC nanoparticles in the Ni-TiN/SiC nanocoatings [27, 28]. The relationship between electric field force and pulse current density can be expressed by Eq. (2):

$$F = \frac{I \times q}{\sigma} \quad (2)$$

where  $I$  denotes the pulse current density,  $q$  is the ionic charge, and  $\sigma$  represents the conductivity of the plating solution.

During PCE deposition of our Ni-TiN/SiC nanocoatings at 2 A/dm<sup>2</sup> pulse current density, the effect of electric field force on TiN and SiC nanoparticles was not very strong, which resulted in low amounts of the particle being incorporated into the coating. Thus, Ni grain growth was not significantly inhibited, which resulted in the formation of numerous large Ni grains [29]. At 4 A/dm<sup>2</sup> electric field force was high enough to decrease layer responsible for the hydrogen evolution layer, which led to the incorporation of significant amounts of TiN and SiC nanoparticles into the coating. These particles provided nucleation sites for Ni grain growth, which in turn, resulted in the formation of smooth, fine-grain and uniform coating. When the coating was prepared at 6 A/dm<sup>2</sup>, substantial amounts of hydrogen bubbles formed at the cathode surface, which increased thickness and hindered deposition of TiN and SiC nanoparticles at the cathode. Therefore, the amount of embedded TiN and SiC nanoparticles in the Ni-TiN/SiC nanocoating was small, which again promoted the formation of large Ni grains [30, 31].

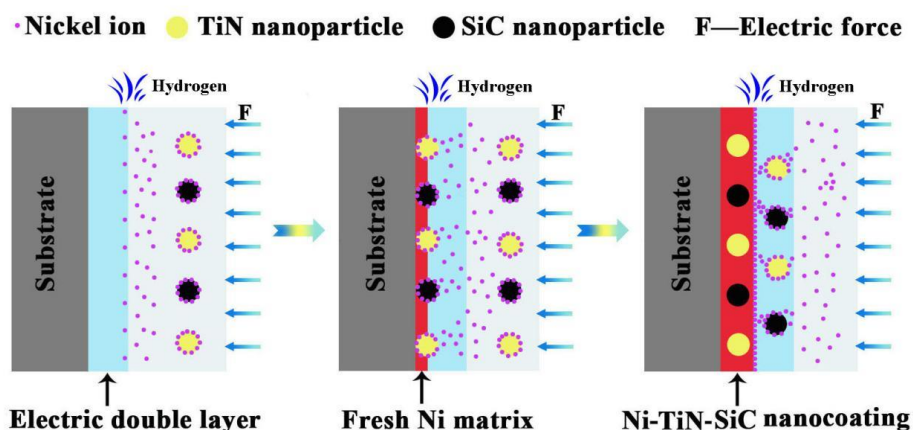


**Figure 7.** The co-deposition mechanism of the nickel ions, TiN nanoparticles and SiC nanoparticles during PCE process.

### 3.5 Microstructure

#### 3.5.1 XRD

XRD analysis of Ni-TiN/SiC nanocoatings prepared at 2, 4 and 6 A/dm<sup>2</sup> showed presence of Ni, SiC and TiN (see Fig. 8). Strong diffractions peaks at 44.8°, 52.2° and 76.7° were attributed to (111), (200) and (220) planes of metallic Ni, respectively. Peaks at 36.6°, 42.6°, and 61.8° correspond to (111), (200) and (220) planes of TiN, respectively. Peaks belonging to (111), (200) and (220) planes of SiC were located at 34.2°, 41.5°, and 59.8°, respectively. The intensity of diffraction peaks of Ni grains was the highest for the coating prepared at 4 A/dm<sup>2</sup>, which confirms our earlier observation that proper current densities can refine Ni grains of the corresponding Ni-TiN/SiC coatings.

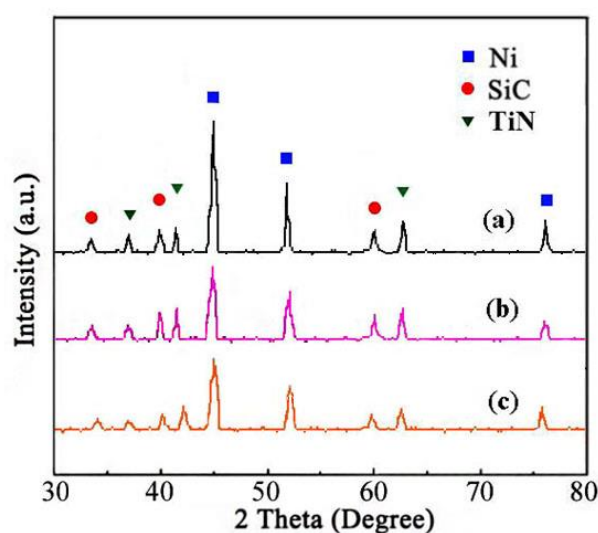


**Figure 8.** XRD patterns of Ni-TiN/SiC nanocoatings produced with different pulse current densities: (a) 2 A/dm<sup>2</sup>, (b) 4 A/dm<sup>2</sup>, and (c) 6 A/dm<sup>2</sup>.

#### 3.5.2 XPS

Cross-sectional XPS analysis showed that TiN and SiC were embedded into the coating (see Fig. 9) obtained at all current densities. However, when 2 A/dm<sup>2</sup> current density was used during coating preparation, fewer TiN and SiC nanoparticles were observed inside the coating (see Fig. 9a). Chemical composition of the coating obtained at 4 A/dm<sup>2</sup> contained 19.6 at% of Ti, 12.1 at% of Si and 53.3 at% of Ni. These contents are higher than for the coatings obtained at 2 and 6 A/dm<sup>2</sup>.

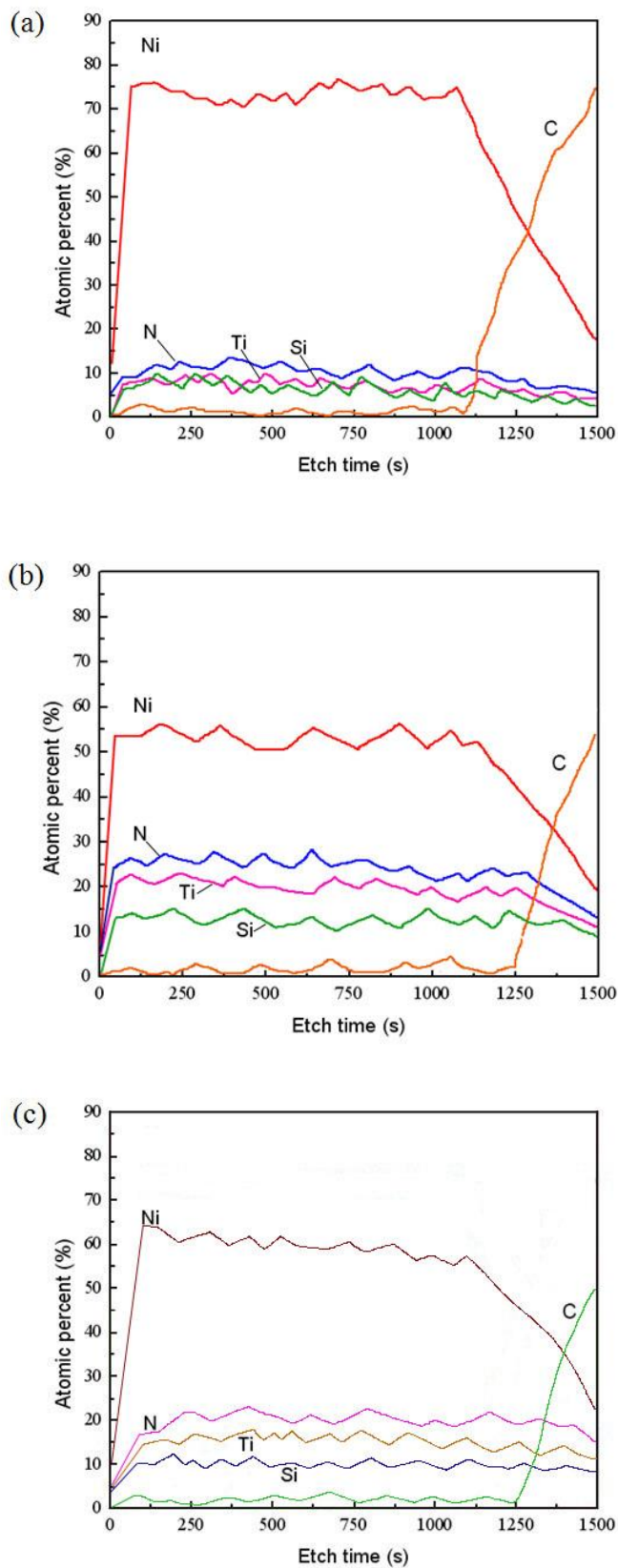


**Figure 9.** XPS cross-sectional profiles of Ni-TiN/SiC nanocoatings produced with different pulse current densities: (a) 2 A/dm<sup>2</sup>, (b) 4 A/dm<sup>2</sup>, and (c) 6 A/dm<sup>2</sup>.

### 3.6 Microhardness test

Microhardness data of the Ni-TiN/SiC nanocoatings prepared at difference pulse current densities are shown in Fig. 10. Microhardness of the Ni-TiN/SiC nanocoating deposited at 4 A/dm<sup>2</sup> was the highest and was equal to 848.1 Hv. The average microhardness of the coating prepared at 2 A/dm<sup>2</sup> was equal to 699.2 Hv. According to the literature [32, 33], nanocoating microhardness should not only depend on TiN and SiC nanoparticle contents (which is expected because TiN and SiC by themselves are very hard materials) but also on their distribution in the coating. Both of these two phenomena were observed in the coating prepared at 4 A/dm<sup>2</sup>. Thus, this coating had the highest microhardness value due to a dispersion–hardening effect.

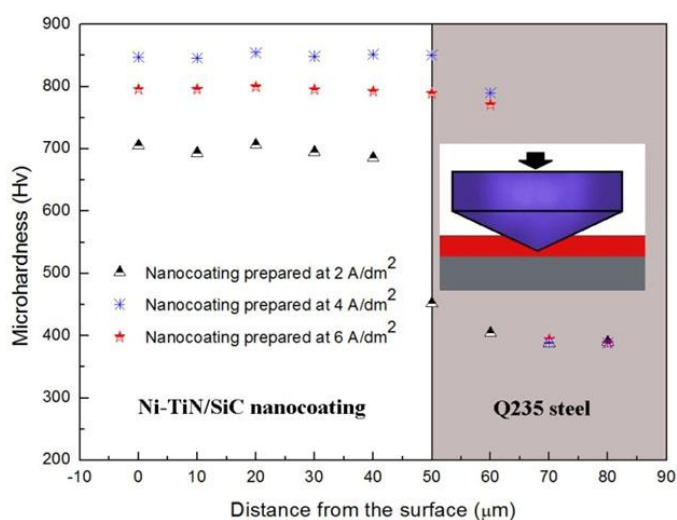
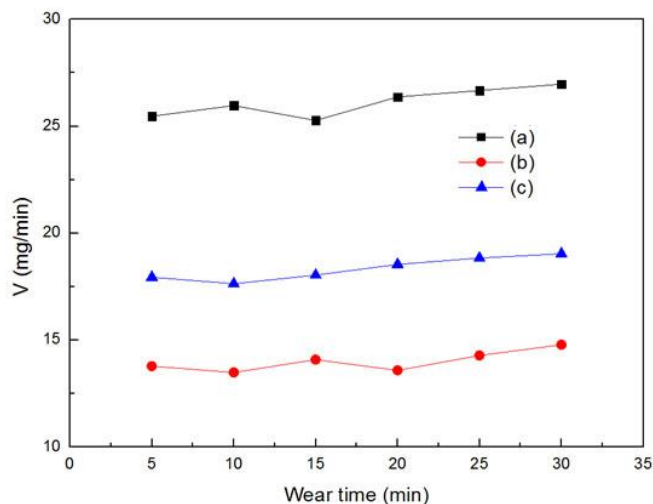


**Figure 10.** Effect of pulse current density on microhardnesses of Ni-TiN/SiC nanocoatings.

### 3.7 Wear test

#### 3.7.1 Wear rate

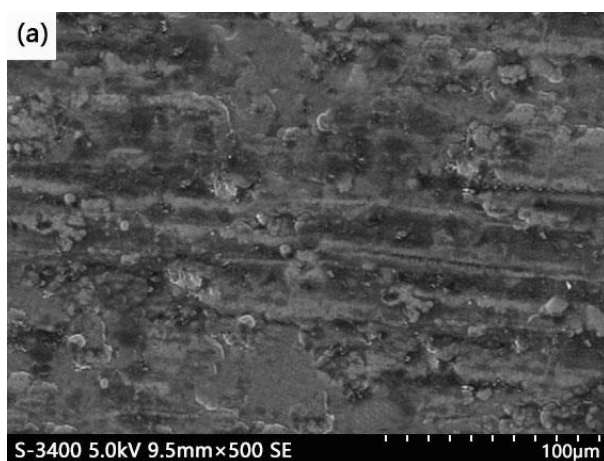
The wear rates of all three nanocoatings were slightly enhanced during wear testing (see Fig. 11). Ni-TiN/SiC nanocoating prepared at 2 A/dm<sup>2</sup> showed the maximum wear rate equal to 27.1 mg/min, while wear rate of the nanocoating prepared at 4 A/dm<sup>2</sup> was only 13.6 mg/min, which indicates its excellent wear resistance.



**Figure 11.** Wear rates of Ni-TiN/SiC nanocoatings produced with different pulse current densities: (a) 2 A/dm<sup>2</sup>, (b) 4 A/dm<sup>2</sup>, and (c) 6 A/dm<sup>2</sup>.

### 3.7.2 Worn surface morphology

Analysis of worn surface morphologies of Ni-TiN/SiC nanocoatings prepared at 2 A/dm<sup>2</sup> after wear tests showed numerous deep grooves and pits (see Fig. 12), which is indicative of severe wear. By contrast, only small scratches were visible on the surface of the coating prepared at 4 A/dm<sup>2</sup>, which confirms its outstanding wear performance. Coating prepared at 6 A/dm<sup>2</sup> also showed large grooves (see Fig. 12).



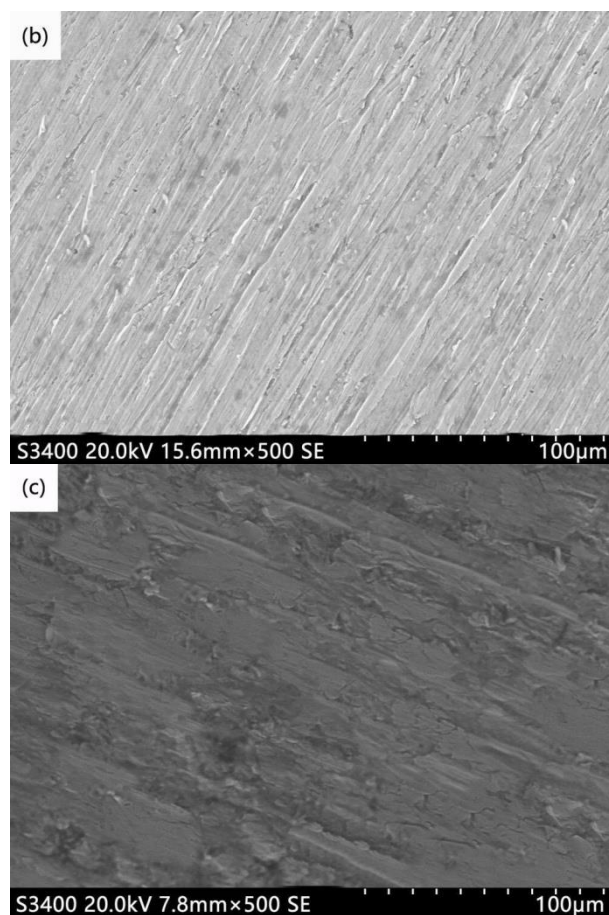


**Figure 12.** SEM images of the worn surface of Ni-TiN/SiC nanocoatings produced with different pulse current densities: (a) 2 A/dm<sup>2</sup>, (b) 4 A/dm<sup>2</sup>, and (c) 6 A/dm<sup>2</sup>.

### 3.7.3 Scheme of wear

Fig. 13 illustrates the wear diagrams of Ni-TiN/SiC nanocoatings deposited at different pulse current densities. The degree of wear resistance of each nanocoating was mainly influenced by its microhardness and microstructure. Because of insufficient formation of TiN and SiC nanoparticles during PCE of Ni-TiN/SiC nanocoatings prepared at 2 and 6 A/dm<sup>2</sup>, their microhardness values were small (see Fig. 13a), and hardened steel barrel could easily tear down large pieces of both of these coating.

At the same time, because Ni-TiN/SiC nanocoating deposited at 4 A/dm<sup>2</sup> showed a uniform and fine microstructure and contained numerous TiN and SiC nanoparticles, which prevented serious coating damage from the hardened steel barrel, only some small scratches were observed on its worn surface (see Fig. 13b).

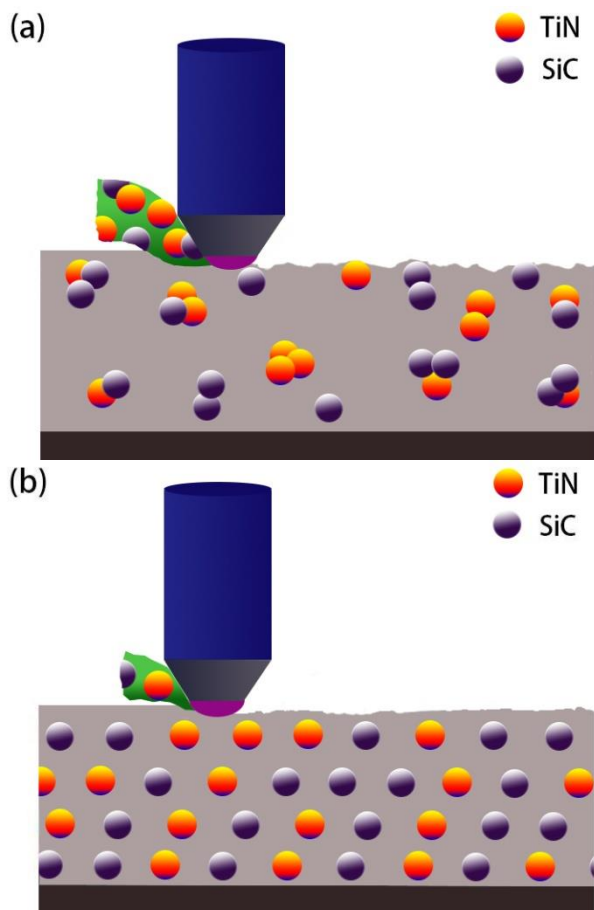


**Figure 13.** Abrasion diagrams of Ni-TiN/SiC nanocoatings produced with different pulse current densities: (a)  $2 \text{ A/dm}^2$  and (b)  $4 \text{ A/dm}^2$ .

### 3.8 Corrosion tests

The potentiodynamic polarization curves of Ni-TiN/SiC nanocoatings deposited at different pulse current densities are shown in Fig. 14. Corresponding corrosion current density ( $i_{corr}$ ) and potential ( $E_{corr}$ ) values are listed in Table 1. The Ni-TiN/SiC nanocoating prepared at  $2 \text{ A/dm}^2$  showed the largest corrosion current density (equal to  $6.91 \times 10^{-5} \text{ A/cm}^2$ ), indicating the worst corrosion resistance. However, Ni-TiN/SiC nanocoating deposited at  $4 \text{ A/dm}^2$  had the smallest corrosion current density equal to  $8.12 \times 10^{-6} \text{ A/cm}^2$ , which indicates the best corrosion resistance.

Fig. 15 shows Nyquist plots of Ni-TiN/SiC nanocoatings prepared at different pulse current densities. Nanocoating prepared at  $2 \text{ A/dm}^2$  showed the lowest impedance ( $Z$ ), which is also indicative of the worst corrosion resistance. Coating prepared at  $4 \text{ A/dm}^2$  had the highest impedance values, which indicates its excellent anti-corrosion ability. Thus, by adjusting pulse current density during PCE, not only morphology and microstructure of the Ni-TiN/SiC coating can be controlled but also its corrosion resistance [34-36]. The favorable microstructure of the coating can minimize and even prevent penetration of the corrosive solution into the coating.

**Table 1.** Electrochemical corrosion data of the Ni-TiN/SiC nanocoatings.

Sample	$I_{corr}$ ( $A \cdot cm^{-2}$ )	$E_{corr}$ (V)
(a)	$6.91 \times 10^{-5}$	-0.625
(b)	$8.12 \times 10^{-6}$	-0.309
(c)	$9.47 \times 10^{-6}$	-0.463

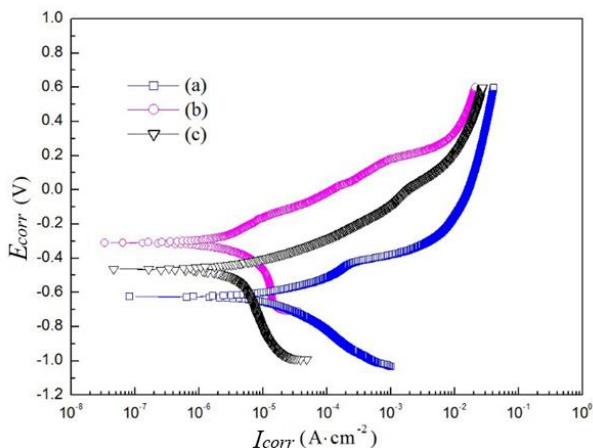


**Figure 14.** Potentiodynamic polarization curves of Ni-TiN/SiC nanocoatings produced with different pulse current densities: (a) 2 A/dm<sup>2</sup>, (b) 4 A/dm<sup>2</sup>, and (c) 6 A/dm<sup>2</sup>.

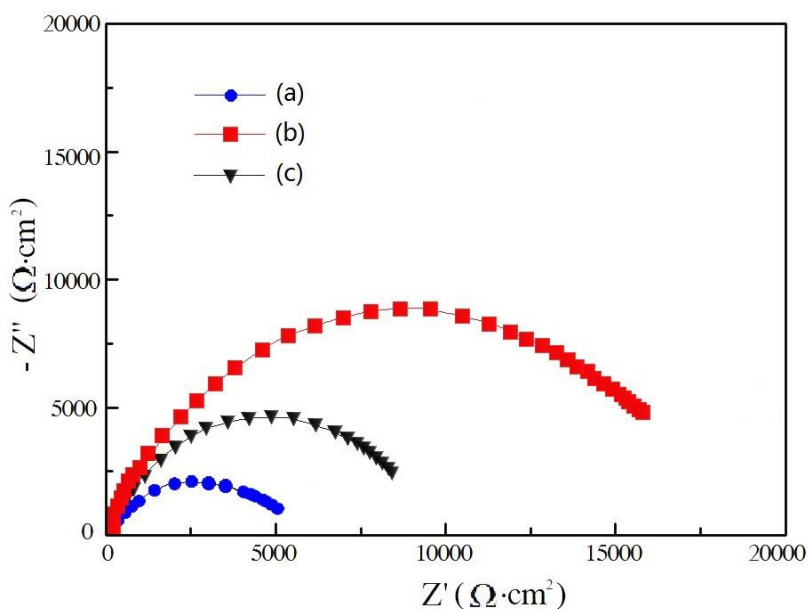


**Figure 15.** Nyquist plots of Ni-TiN/SiC nanocoatings produced with different pulse current densities: (a) 2 A/dm<sup>2</sup>, (b) 4 A/dm<sup>2</sup>, and (c) 6 A/dm<sup>2</sup>.

#### 4. CONCLUSION

(1) Smooth and uniform Ni-TiN/SiC nanocoating with fine grains was obtained during PCE at 4 A/dm<sup>2</sup> pulse current density. At 2 A/dm<sup>2</sup>, some TiN and SiC nanoparticles formed on the Ni-TiN/SiC

nanocoating surface, while during PCE at 4 A/dm<sup>2</sup> these nanoparticles (with average sizes equal to 45.9 and 37.2 nm, respectively) were mostly incorporated into the coating.

(2) All coatings contained Ni, SiC and TiN crystalline phases. However, Ni-TiN/SiC nanocoating prepared at 2 A/dm<sup>2</sup> showed fewer TiN and SiC nanoparticles than those prepared at 4 and 6 A/dm<sup>2</sup>. The highest concentration of Ti (19.6 at%), Si (12.1 at%) and Ni (53.3 at%) were obtained throughout the cross-section of the Ni-TiN/SiC nanocoating deposited at 4 A/dm<sup>2</sup>.

(3) Microhardness of Ni-TiN/SiC nanocoating deposited at 4 A/dm<sup>2</sup> was equal to 848.1 Hv, which is higher than for other coatings tested in this work. The wear rate of Ni-TiN/SiC nanocoating prepared at 4 A/dm<sup>2</sup> was only 13.6 mg/min, indicating its excellent wear resistance. Only some small scratches were observed on the surface of this nanocoating, which testifies of its excellent wear performance.

(4) The Ni-TiN/SiC nanocoating prepared at 2 A/dm<sup>2</sup> showed the largest corrosion current density (equal to 6.91×10<sup>-5</sup> A/cm<sup>2</sup>), indicating the worst corrosion resistance. However, Ni-TiN/SiC nanocoating deposited at 4 A/dm<sup>2</sup> had the smallest corrosion current density equal to 8.12×10<sup>-6</sup> A/cm<sup>2</sup>, which indicates the best corrosion resistance.

#### ACKNOWLEDGEMENT

This work has been supported by the National Natural Science Foundation of China (Grant Nos. 51974089, 51674090), Natural Science Foundation of Heilongjiang Province of China (Grant No. LC2018020), Innovative and Entrepreneurship Training Program for College Students in Heilongjiang Province (Grant No. 201910220060).

#### References

1. X. Li, J. Feng, Y. Jiang, H. Lin and J. Feng, *Ceram. Int.*, 44 (2018) 19143.
2. Y. Yang, Y. Chen, X. Du, S. Feng, and Z. Zhang, *Int. J. Electrochem. Sci.*, 13 (2018) 384.
3. S. Tamariz, D. Martin and N. Grandjean, *J. Cryst. Growth.*, 476 (2017) 58.
4. H. Zhou, W. Wang, Y. Gu, X. Fang and Y. Bai, *Strength. Mater.*, 1 (2017) 1.
5. C. Wang, L.D. Shen, M.B. Qiu, Z.J. Tian and W. Jiang, *J. Alloy. Compd.*, 727 (2017) 269.
6. T. Mikolajczyk, and B. Pierozynski, *Int. J. Electrochem. Sci.*, 13 (2018) 621.
7. M. Wu, W. Jia and P. Lv, *Procedia. Eng.*, 174 (2017) 717.
8. Y. Chen, Y. Hao, W. Huang, Y. Ji, W. Yang, X. Yin, Y. Liu and X. Ling, *Surf. Coat. Tech.*, 310 (2017) 122.
9. B. Li, *Int. J. Electrochem. Sci.*, 12 (2017) 7017.
10. Z. Xu, and Y. Chen, *J. Nanosci. Nanotechno.*, 13 (2013) 1456.
11. B. Li, W. Zhang, W. Zhang and Y. Huan, *J. Alloy. Compd.*, 702 (2017) 38.
12. Q. Fan, Y. Gao, Y. Zhao, Q. Yang, L. Guo and L. Jiang, *Mater. Lett.*, 215 (2018) 242.
13. S. Qi, X. Li, Z. Zhang and H. Dong, *Thin. Solid. Films.*, 644 (2017) 106.
14. L. Wu, J.E. Graves and A.J. Cobley, *Mater. Lett.*, 217 (2018) 120.
15. M. Shourgeshty, M. Aliofkhaezai and A. Karimzadeh, *Surf. Eng.*, 35 (2019) 167.
16. R. M. Reddy, B.M. Praveen and C.M.P. Kumar, *Surf. Eng. Appl.*, 53 (2017) 179.
17. M. Aghazadeh, M.G. Maragheh, M.R. Ganjali and P. Norouzi, *Syn. React. Inorg. Met.*, 47 (2017) 1085.
18. F. Xia, W. Jia, M. Jiang, W. Cui and J. Wang, *Ceram. Int.*, 43 (2017) 14623.
19. Y. Wang, Q. Zhou, K. Li, Q. Zhong, and Q.B. Bui, *Ceram. Int.* 41 (2015) 79.

20. A. Hefnawy, N. Elkhoshkhany and A. Essam, *J. Alloy. Compd.*, 735 (2018) 600.
21. F. Xia, W. Jia, C. Ma and J. Wang, *Ceram. Int.*, 44 (2018) 766.
22. M. Ebadi, W.J. Basirun and Y. Alias, *J. Chem. Sci.*, 122 (2010) 279.
23. P. Colomban and G. Gouadec, *J. Raman. Spectrosc.*, 38 (2007) 598.
24. H. Lan, C. Ma, Y. Li, and F. Xia, *Ordinance Mater. Sci. Eng.*, 38 (3) (2015) 52. (In Chinese)
25. B. Li, D. Li, W. Chen, Y. Liu, J. Zhang, Y. Wei, W. Zhang and W. Jia, *Ceram. Int.*, 45 (2019) 4870.
26. B. Bahadormanesh, A. Dolati and M.R. Ahmadi, *J. Alloy. Compd.*, 509 (2011) 9406.
27. F. Xia, J. Tian, C. Ma, M. Potts and X. Guo, *J. Appl. Phys.*, 116 (2014) 234301.
28. B. Bakhit, A. Akbari, F. Nasirpouri, and M.G. Hosseini, *Appl. Surf. Sci.* 307 (2014) 351.
29. V. Ezhilselvi, J. Nithin and J.N. Balaraju, *Surf. Coat. Tech.*, 288 (2016) 221.
30. F.F. Xia, W.C. Jia, C.Y. Ma, R. Yang, Y. Wang and M. Potts, *Appl. Surf. Sci.*, 434 (2018) 228.
31. C. Ma, W. Yu, M. Jiang, W. Cui and F. Xia, *Ceram. Int.*, 44 (2018) 5163.
32. F. Xia, J. Tian, W. Wang and Y. He, *Ceram. Int.*, 42 (2016) 13268.
33. C. Ma, M. Jiang and F. Xia, *Surf. Rev. Lett.*, 24 (2016) 17500631.
34. G. Zhao, Y. Wei and L.I. Jing, *J. Chin. Soc. Corros. Rrot.*, 35 (2015) 69.
35. M. Zhu, C.W. Du and X. G. Li, *J. Univ. Sci. Technol. B.*, 36 (2014) 1077.
36. F. Liang, Z. Wang, J. Sunarso, J. Mao, and W. Zhou, *Int. J. Hydrogen Energy*, 43(1) (2018) 53.

© 2020 The Authors. Published by ESG ([www.electrochemsci.org](http://www.electrochemsci.org)). This article is an open access article distributed under the terms and conditions of the Creative Commons Attribution license (<http://creativecommons.org/licenses/by/4.0/>).